Headache
© 2014 American Headache Society

ISSN 0017-8748
doi: 10.1111/head.12459
Published by Wiley Periodicals, Inc.

Research Submissions

Changes of Migraine-Related White Matter Hyperintensities After 3 Years: A Longitudinal MRI Study

Szilvia Erdélyi-Bótor, MD; Mihály Aradi, MD, PhD; David Olayinka Kamson, MD; Norbert Kovács, MD, PhD; Gábor Perlaki; Gergely Orsi, PhD; Szilvia Anett Nagy; Attila Schwarcz, MD, PhD; Tamás Dóczi, MD, DSc; Sámuel Komoly, MD, DSc; Gabriella Deli, MD; Anita Trauninger, MD, PhD; Zoltán Pfund, MD, PhD

Objective/Background.—The aim of this longitudinal study was to investigate changes of migraine-related brain white matter hyperintensities 3 years after an initial study. Baseline quantitative magnetic resonance imaging (MRI) studies of migraine patients with hemispheric white matter hyperintensities performed in 2009 demonstrated signs of tissue damage within the hyperintensities. The hyperintensities appeared most frequently in the deep white matter of the frontal lobe with a similar average hyperintensity size in all hemispheric lobes. Since in this patient group the repeated migraine attacks were the only known risk factors for the development of white matter hyperintensities, the remeasurements of migraineurs after a 3-year long follow-up may show changes in the status of these structural abnormalities as the effects of the repeated headaches.

Methods.—The same patient group was reinvestigated in 2012 using the same MRI scanner and acquisition protocol. MR measurements were performed on a 3.0-Tesla clinical MRI scanner. Beyond the routine T1-, T2-weighted, and fluid-attenuated inversion recovery imaging, diffusion and perfusion-weighted imaging, proton magnetic resonance spectroscopy, and T1 and T2 relaxation time measurements were also performed. Findings of the baseline and follow-up studies were compared with each other.

Results.—The follow-up proton magnetic resonance spectroscopy studies of white matter hyperintensities showed significantly decreased N-acetyl-aspartate (median values 8.133 vs 7.153 mmol/L, $P = .009$) and creatine/phosphocreatine (median values 4.970 vs 4.641 mmol/L, $P = .015$) concentrations compared to the baseline, indicating a more severe axonal loss and glial hypocellularity with decreased intracellular energy production. The diffusion values, the T1 and T2 relaxation times, and the cerebral blood flow and volume measurements presented only mild changes between the studies. The number (median values 21 vs 25, $P < .001$) and volume (median values 0.896 vs 1.140 mL, $P < .001$) of hyperintensities were significantly higher in the follow-up study. No changes were found in the hemispheric and lobar distribution of hyperintensities. An increase in the hyperintensity size of preexisting lesions was much more common than a decrease (median values 14 vs 5, $P = .004$). A higher number of newly developed hyperintensities were detected than disappeared ones (130 vs 22), and most of them were small (<.034 mL). Small white matter hyperintensities in patients with a low migraine attack frequency had a higher chance to disappear than large white matter hyperintensities or white matter hyperintensities in patients with a high attack frequency (coefficient: −0.517, $P = .034$).

Conclusions.—This longitudinal MRI study found clinically silent brain white matter hyperintensities to be predominantly progressive in nature. The absence of a control group precludes definitive conclusions about the nature of these changes or if their degree is beyond normal aging.

From the Department of Neurology, University of Pécs, Pécs, Hungary (S. Erdélyi-Bótor, D.O. Kamson, N. Kovács, G. Perlaki, G. Orsi, S. Komoly, G. Deli, A. Trauninger, and Z. Pfund); Diagnostic Center of Pécs, Pécs, Hungary (M. Aradi, G. Perlaki, G. Orsi, and S.A. Nagy); MTA-PTE Clinical Neuroscience MR Research Group, Pécs, Hungary (G. Perlaki, G. Orsi, A. Schwarcz, and T. Dóczi); Department of Radiography, Faculty of Health Sciences, University of Pécs, Pécs, Hungary (S.A. Nagy); Department of Neurosurgery, University of Pécs, Pécs, Hungary (A. Schwarcz and T. Dóczi).

Address all correspondence to Z. Pfund, 7623 Pécs, Rét u. 2. Hungary, email: pfund.zoltan@pte.hu

Accepted for publication June 26, 2014.

Key words: migraine, brain white matter hyperintensity, quantitative 3.0-Tesla MRI, volumetry, longitudinal analysis

Abbreviations: ^{1}H-MRS proton magnetic resonance spectroscopy, ADC apparent diffusion coefficient, CHESS chemical shift-selective sequence, Cho choline, Cr creatine/phosphocreatine, DWI diffusion-weighted imaging, FLAIR fluid-attenuated inversion recovery, FLASH fast low angle shot, Glx glutamate/glutamine, Lac lactate, mI myo-inositol, NAA N-acetyl-aspartate, NAWM normal-appearing white matter, PRESS point resolved spectroscopy sequence, PWI perfusion-weighted imaging, rCBF relative cerebral blood flow, rCBV relative cerebral blood volume, ROI region of interest, WMH white matter hyperintensity, WML white matter lesion

(*Headache* 2015;55:55-70)

Migraine is a primary headache disorder with episodic headache attacks.[1] Migraine is an independent risk factor for brain white matter lesions (WMLs) and silent posterior circulation territory infarcts.[2-7] The presence of these lesions does not correlate with age.[8,9] The pathogenesis of lesion development is not completely known, and findings of histopathological investigations of WMLs are not available in migraine. Both the disease duration and the attack frequency have an important role in the lesion evolution, and the effects of comorbid diseases may also lead to the development of lesions.[10,11] Different attack-related pathomechanisms have been considered in the formation of WMLs.[10,11] Among these, the effects of repeated intracerebral hemodynamic changes, including oligemia and focal hypoperfusion with tissue ischemia have been proposed.[4,12]

Our previous quantitative magnetic resonance imaging (MRI) study of chronic supratentorial white matter hyperintensities (WMHs) in migraine patients demonstrated tissue damage with axonal loss, decreased glial cell density with impaired energy metabolism, an enlarged extracellular space with an increased extracellular water fraction and decreased blood flow and volume.[13] Since the radiological features of these MRI-visible hyperintensities were similar to those detected in chronic WMLs with ischemic origin,[14-16] and histopathologic findings of WMHs in elderly patients showed reduced vascular and blood–brain barrier integrity,[17] our findings indicated that these WMHs could be the consequence of a microvascular ischemic injury in migraine.[13] The number, volume, and location of the WMHs were also investigated in the same patient group.[18] The WMHs appeared most frequently in the deep white matter in the anterior circulation territory, mainly in the frontal and parietal lobes, with a similar average WMH size in all hemispheric lobes.[18]

Since the advanced MRI methods provide an opportunity to reinvestigate the previously studied migraine group using the same MR system and acquisition protocol, we repeated the same measurements exactly 3 years after the end of the initial study to determine whether the recurrent headache attacks were associated with a progression of WMHs.

PATIENTS AND METHODS

Patients.—Seventeen migraine patients (15 females and 2 males, mean age ± standard deviation [SD] 47.0 ± 11.2 years, age range 22-68 years) with previously discovered brain WMHs were prospectively enrolled in the study at the Outpatient Headache Department of the Department of Neurology, Medical School, University of Pécs, Hungary. The patients were divided into 2 subgroups: 10 patients fulfilled the International Headache Society classification criteria[1] of migraine without aura and 7 patients of migraine with aura (Table 1). None of the included migraine patients had other types of headaches. All selected patients were chosen if they had

Funding: This work was supported by grants from EEA/Norwegian Financial Mechanism HU 0114 – "Save what can be saved" – applied neurological research using high-field magnetic resonance imaging and by TÁMOP-4.2.1/B, TÁMOP.4.2.1/B-10/2/KONV-2010-0002 and Hungarian Brain Research Program – Grant No. KTIA_13_NAP-A-II/10. A.S. and N.K. were supported by the Bolyai Scholarship of the Hungarian Academy of Science. N.K. was supported by OTKA PD 103964.

Conflict of Interest: None.

Table 1.—Clinical and White Matter Hyperintensity Data of Migraine Patients

			Clinical Aspects of Migraine					White Matter Hyperintensities (WMHs)							
					Attack Frequency/Month			Total Number of WMHs			Comparison Between 2009 and 2012 (Number of WMHs)				
Patient	Gender	Age (years) 2012	Migraine Type	Disease Duration (years) 2012	2009	2012	Change	2009	2012	Change	Unchanged Size	Increase in Size	Decrease in Size	Disappeared	Newly Developed
1	Female	22	With aura	8	3	3	Unchanged	17	25	8	0	16	1	0	8
2	Female	28	Without aura	13	8	8	Unchanged	7	11	4	0	2	5	0	4
3	Female	35	Without aura	17	2	1	Improved	21	23	2	1	10	6	4	6
4	Female	41	Without aura	31	2,5	4	Worsened	46	55	9	0	37	7	2	11
5	Female	43	Without aura	23	3	2	Improved	5	5	0	1	3	1	0	0
6	Male	44	Without aura	24	2	2	Unchanged	54	65	11	0	41	7	6	17
7	Female	46	Without aura	28	10	10	Unchanged	5	9	4	0	2	1	2	6
8	Female	46	With aura	27	1	1	Unchanged	14	18	4	0	10	4	0	4
9	Female	47	Without aura	29	3,5	3,5	Unchanged	22	27	5	2	11	9	0	5
10	Female	47	With aura	31	6	4	Improved	28	33	5	5	17	6	0	5
11	Female	48	With aura	28	4	4	Unchanged	39	46	7	2	23	14	0	7
12	Female	49	With aura	29	5	5	Unchanged	2	7	5	0	1	1	0	5
13	Female	50	Without aura	28	8	8	Unchanged	12	23	11	0	9	3	0	11
14	Female	51	Without aura	37	4	4	Unchanged	31	39	8	1	19	11	0	8
15	Male	54	With aura	40	1	1	Unchanged	21	33	12	0	14	5	2	14
16	Female	56	Without aura	38	2,5	1,5	Improved	20	23	3	0	15	5	0	3
17	Female	68	With aura	48	0,5	0.5	Unchanged	46	56	10	1	34	5	6	16

hemispheric WMHs on fluid-attenuated inversion recovery (FLAIR) and T2-weighted images without hypointensity on T1-weighted scans. Further, to gain more accurate information from the WMHs by the MR imaging protocol, migraineurs were chosen for having at least 1 large signal abnormality with homotopic, normal-appearing white matter (NAWM) contralaterally. All selected patients underwent detailed clinical investigations to exclude the presence of any medical comorbidity (hypertension, diabetes, hyperlipidemia, thyroid gland disorder, hyperhomocystinemia, hyperuricemia, elevated C-reactive protein, smoking, kidney disease, systemic autoimmune disease, cardiac embolization source), which may itself cause brain WMHs. All patients lacked such comorbidities. All included migraineurs underwent the same brain magnetic resonance imaging (MRI) protocol performed in 2009 (baseline study)[13,18] and 2012 (follow-up study). All MRI studies were performed in a headache-free state, and the patients were not on migraine prophylactic treatments at the time of the scans and during the 3 year-long follow-up period. Patients used eletriptan and nonsteroidal anti-inflammatory drugs (ibuprofen and diclofenac) as acute treatment. All migraineurs were symptom free at the beginning of the study, and changes in their physical status were not detected during the observation period. The headache frequency of most patients remained unchanged in the follow-up period (Table 1).

All participants provided informed consent. Studies were performed in accordance with the approval of the Regional Research Ethics Committee of the Medical Center, Pécs.

MR Scanning Protocol and Data Analysis.—A 3.0-Tesla clinical MRI scanner (Magnetom TIM Trio, Siemens Medical Solutions, Erlangen, Germany) with a 12-channel phased-array head coil was used for MR measurements. Routine T1-, T2-weighted, and FLAIR imaging was performed, and additionally, diffusion and perfusion-weighted imaging (DWI and PWI), proton magnetic resonance spectroscopy (^{1}H-MRS), and T1 and T2 relaxation time measurements were performed, as well. For standard and accurate axial slice positioning, the anterior and posterior commissural line (AC-PC line) was used as a reference for T2-weighted and FLAIR images, while perfusion and diffusion images were acquired parallel to the anterior cranial base. The sequence parameters are listed in Table 2.

One hundred volumes were consecutively acquired for perfusion imaging, and contrast agent

Table 2.—Magnetic Resonance Parameters for Morphological and Quantitative Imaging Sequences

	Sequences*				
Parameters	T1W-FLASH Sagittal	T2W-TSE Axial	FLAIR Axial	SE-EPI Diffusion Axial	GE-EPI Perfusion Axial
Repetition time (ms)	300	6000	15,710	4000	1400
Echo time (ms)	2.46	93	105	119	33
Inversion time (ms)	–	–	2750	–	–
Number of slices	27	30	100	20	20
Flip angle (degree)	88	120	120	90	68
Slice thickness (mm)	4	4	1.5	3.5	3
Interslice gap (%)	30	20	0	0	33
Field of view (mm^2)	220 × 220	193 × 220	220 × 220	188 × 250	210 × 210
Matrix	256 × 320	280 × 320	192 × 192	144 × 192	176 × 176
Bandwidth (Hz/pixel)	330	220	400	1302	1150
Fat saturation	off	off	off	on	on

*All of the imaging sequences were acquired in 2-dimensional mode.
– = not measurable; EPI = echo planar imaging; FLAIR = fluid attenuated inversion recovery; FLASH = fast low angle shot; GE = gradient echo; SE = spin echo; TSE = turbo spin echo.

was administered after the 20th volume. A 0.1 mL/body weight amount of gadolinium solution contrast agent (gadopentetate dimeglumin, Bayer Schering Pharma AG, Berlin, Germany) was given at a 5 mL/second flow rate, and a 30 mL saline flush was used for washing in, also at a 5 mL/second flow rate. Both contrast and saline administration was carried out using a Medrad power injector.

Spectroscopy.—To avoid possible interference, spectroscopy was performed prior to contrast agent administration. A voxel of $12 \times 12 \times 12$ mm^3 was positioned on a preselected WMH before ^{1}H-MRS acquisition, and 2 voxels were placed in every migraine patient: 1 in the selected WMH and 1 in the contralateral, homotopic, NAWM. In total, 24 frontal, 2 frontoparietal, 4 parietal, and 4 occipital voxels were placed in both the baseline and the follow-up studies. Voxels were positioned on both T2-weighted and FLAIR images. Water suppression was carried out using a chemical shift-selective sequence (CHESS) pulse, and after manual shimming and water suppression adjustment, fully relaxed short-echo time proton MR spectra (point resolved spectroscopy sequence [PRESS], TR/TE = 6000/30 ms, averages = 128, bandwidth = 1200 Hz, vector size = 1024) were acquired. A reference water signal for the calibration of metabolite concentration was also acquired at the end of the MRS by turning off the water suppression.

Water signal T1 and T2 parameters were determined for each spectroscopy voxel after obtaining the metabolite spectra. T1 was measured using the saturation recovery method in which 6 data points were collected, and only the TR was changed between each data point acquisition, using the PRESS sequence: TR = 490, 900, 1400, 2000, 3000, 4000 ms, TE = 30 ms, averages = 1, water signal suppression turned off, bandwidth = 2500 Hz, vector size = 1024, 4 preparation scans. T2 was obtained by measuring 6 data points with parameters differing only in echo times using the PRESS sequence: TR = 3000 ms, TE = 30, 60, 90, 120, 180, 240 ms, 1 accumulation, water signal suppression turned off, bandwidth = 2500 Hz, vector size = 1024, 4 preparation scans.

Data Processing.—To calculate the T1 relaxation time for each spectroscopy voxel from the acquired water signals with different repetition times, the following exponential fit was applied:

$$M = M_0 * [1 - \exp(-TR/T_1)] \quad (1)$$

where M is the actual water signal, M_0 is the water signal at thermal equilibrium, and TR is the repetition time.

For T2, the relaxation time for each spectroscopy voxel was calculated from the acquired water signals with different echo times assuming mono-exponential signal decay:

$$M = M_0 * \exp(-TE/T_2) \quad (2)$$

where M is the actual water signal, M_0 is the water signal at thermal equilibrium, and TE is the echo time. The unsuppressed water signals were post-processed on a Siemens Leonardo workstation using the Siemens spectroscopy software. Only Fourier transformation and phase correction on the measured signals were applied, no filters or any other corrections were used. The integral of the fitted water signal was used for the T1 and T2 fitting.

The apparent diffusion coefficient (ADC) values were calculated by drawing freehand regions of interest (ROIs) on b0 images to selectively cover the preselected WMHs. Within each ROI, the mean signal intensities for the b0, b500, and b1000 images were monoexponentially fitted using the following equation:

$$M = M_0 * \exp(-b * ADC) \quad (3)$$

where M is the measured signal intensity in the presence of diffusion sensitization, M_0 is the signal intensity in the absence of diffusion sensitization, b is the b-value, and ADC is the ADC value. T1, T2, and diffusion data processing was carried out using Matlab software's curve fitting toolbox and a self-written program code (The MathWorks Inc., Natick, MA, USA) software.

For the quantitative analysis of metabolite concentrations, the spectroscopic raw data were post-processed using the LC Model (Stephen Provencher Inc., Oakville, Ontario, Canada).[19] The concentrations of N-acetyl-aspartate (NAA), glutamate/glutamine

(Glx), creatine/phosphocreatine (Cr), choline compounds (Cho), myo-inositol (mI), and lactate (Lac) were determined.

A Siemens Leonardo Workstation was used for perfusion analysis utilizing the Siemens Perfusion software (Siemens Medical Solutions, Erlangen, Germany). The relative cerebral blood flow (rCBF) and relative cerebral blood volume (rCBV) were calculated. The arterial input function was determined by an experienced radiologist. The free-hand ROIs were drawn on hyperintense lesions on T2* images by referring to T2-weighted and FLAIR images. Afterward, these ROIs were copied and used at the same slice of the calculated rCBF and rCBV maps. A control area was also selected for each patient on the side contralateral to the lesion in order to have white matter area without signal abnormality. For comparisons of baseline and follow-up rCBF and rCBV data, WMH/NAWM rCBF and WMH/NAWM rCBV ratios were calculated.

Identification of WMHs.—WMHs were considered if they were visible as hyperintense areas on T2-weighted and FLAIR images without hypointensity on T1-weighted scans, were larger than 3 mm and appeared in at least 2 consecutive slices.[20] Each MR scan was analyzed by at least 2 independent investigators. All detected hyperintensities were counted, and their volumes were measured. One large hyperintensity was also investigated in each patient using DWI, PWI 1H-MRS, and T1 and T2 relaxation time measurements. For perfect comparisons of large WMHs, the same ROIs (ie, same anatomical location and size) were used in the follow-up study. The largest diameters of the investigated signal abnormalities ranged between 6-22 mm and appeared in at least 3 consecutive slices on FLAIR images.

Volumetry.—3D Slicer was used as the software evaluation tool for the images (http://www.slicer.org, Version 3.6).[21] Hemispheric WMHs were marked manually in order to create label maps, and the volume of the label maps was determined using 3D Slicer's Label Statistics module. A 3D model was created of each lesion label map and of each patient's gray matter to aid in the differentiation of lobe boundaries and the localization of hyperintensities (Fig. 1). Borders were defined by aligning orthogonal planes along the anatomical boundaries of lobes as follows: (1) frontal lobe: the central and lateral sulci; (2) parietal lobe: central sulcus, a horizontal plane elongating the lateral sulcus, a vertical plane between the parieto-occipital sulcus and the parieto-occipital incisure; (3) temporal lobe: lateral sulcus and a horizontal plane elongating the lateral sulcus, a vertical plane between the parieto-occipital sulcus and the parieto-occipital incisure; (4) occipital lobe: a vertical plane between the parieto-occipital sulcus and the parieto-occipital incisure. WMHs were counted, their

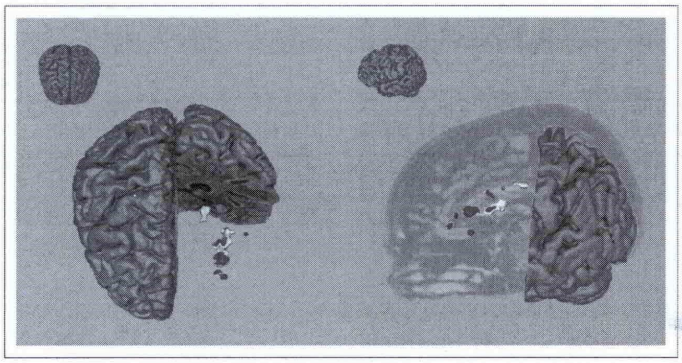

Fig 1.—Superior and sagittal views of a patient's cortical surface and white matter hyperintensities rendered in 3D. On this figure, the left frontal lobe was removed to reveal the white matter hyperintensities from the baseline study (dark), and these are overlaid with the hyperintensities detected in the follow-up study (bright semi-transparent).

cerebral and lobar volumes were measured (mL), and the average size of the individual hyperintensities was calculated (mL) for each patient. Based on their volumes, hyperintensities were categorized as small (0-33 percentiles), medium-sized (33-66 percentiles), or large (66-100 percentiles). The hemispheres and the left and right pair of lobes (frontal, parietal, temporal, and occipital) were not separated. The hyperintensities were also investigated by their intrahemispheric locations: subcortical with U-fiber involvement, deep white matter, periventricular, and corpus callosum. To increase the reliability of hyperintensity measurements, the 2 FLAIR images obtained at different times were aligned to each other for all subjects using FMRIB's Linear Image Registration Tool[22] with 6 degrees-of-freedom (rigid-body transformation). Both FLAIR images were then resampled into the space halfway between the 2 to ensure that both of them are subjected to the same amount of interpolation-related blurring. This halfway registration is recommended for longitudinal analysis, instead of simple registration of 1 time point to the other (eg, registering the later time point to the earlier).[23]

Statistical Analysis.—All statistical tests were performed using the IBM SPSS Software (version 20, SPSS Inc, Chicago, IL). To test normality the Kolmogorov–Smirnov and the Shapiro–Wilk tests were applied. Since the variables did not follow the normal distribution, nonparametric tests were used in subsequent analyses. First, we compared the results of patients with and without aura to each other (Mann–Whitney test). Because we did not find any statistical differences between these 2 groups, we performed all subsequent statistical analyses on the combined group of patients. To compare the baseline and follow-up values, Wilcoxon's test was applied. Spearman's correlation was performed to investigate the relationship between the number of migraine attacks and the hyperintensity number. Changes (increase vs decrease in size) between hyperintensity categories (small, medium, large) were evaluated by Pearson's chi-square test. To reduce type 1 error, the Bonferroni correction was applied. The level of statistical significance was set at ≤.05 for the adjusted *P* values.

RESULTS

Investigation of Large WMHs.—*Diffusion Analysis.*—Although the follow-up studies showed higher ADC values, the differences between the baseline and follow-up studies were not statistically significant (Table 3, Fig. 2A). Out of 17 migraineurs, 12 patients had higher ADC values in the follow-up study.

T1 and T2 Relaxation Time Measurements.—Only mild differences were found between the baseline and follow-up studies (Table 3, Fig. 2B). Higher T1 and T2 values were detected in 9 migraine patients during the follow-up measurements.

^{1}H-MRS Studies.—As compared to the baseline values, significantly decreased NAA ($P = .009$) and Cr ($P = .015$) concentrations were detected in the follow-up study (Table 3, Fig. 2C). Of 17 patients, 15 patients had lower metabolite concentrations, while in the remaining 2 patients, no changes were detected. The other investigated metabolites (Glx, Cho, mI), showed no significant interval changes (Table 3, Fig. 2C). A Lac peak was not present either in the baseline or in the follow-up study in any of the patients.

Perfusion Analysis.—The comparison of the baseline and follow-up studies showed only nonsignificant changes in WMH/NAWM rCBF and WMH/NAWM rCBV ratios (Table 3, Fig. 2D). Lower WMH/NAWM rCBF and WMH/NAWM rCBV ratios were found in 11 and 12 patients, respectively, in the follow-up study.

Investigation of All Hemispheric WMHs.—*Number and Locations of WMHs.*—A significantly higher number of WMHs was detected in the follow-up study than in the baseline study (498 vs 370, $P < .001$; Table 3, Fig. 3A). A higher hyperintensity count was found in all 4 lobes in the follow-up study, and except the occipital lobe, these differences were statistically significant (frontal $P < .001$, parietal $P = .018$, temporal $P = .021$; Table 3, Fig. 3A). Analyzing the lobar distribution of WMHs, the same pattern was found in both studies with the highest number of hyperintensities in the frontal lobe followed by the parietal, temporal, and occipital lobes (Table 3, Fig. 3A). The WMHs were located most frequently in the deep white matter followed by the

Table 3.—Results of the Measured Variables and the Statistical Differences Between the Studies

Investigated Parameters	Baseline Study			Follow-Up Study			Bonferroni-Adjusted *P* Values
	Median	25 Percentile	75 Percentile	Median	25 Percentile	75 Percentile	
ADC ($\times 10^{-4}$ mm^2/s)	9.694	8.508	10.905	10.024	9.460	11.307	*.579*
T1 (ms)	1027	981	1163	1054.9	984.2	1157	*1.000*
T2 (ms)	79.27	75	91.82	79.8	76.3	89.2	*1.000*
NAA (mmol/L)	8.133	6.724	8.659	7.153	6.837	8.115	*.009*
Glx (mmol/L)	8.553	7.176	8.93	7.63	6.161	8.572	*.372*
Cr (mmol/L)	4.97	4.444	5.205	4.641	4.278	5.006	*.015*
Cho (mmol/L)	1.535	1.351	1.817	1.459	1.409	1.598	*1.000*
mI (mmol/L)	4.805	4.103	5.077	4.543	4.229	5.415	*1.000*
WMH/NAWM rCBF	0.665	0.646	0.815	0.678	0.565	0.795	*1.000*
WMH/NAWM rCBV	0.757	0.662	0.898	0.722	0.624	0.789	*.420*
Cerebral WMH number	21	12	31	25	18	39	*.001*
Frontal lobe WMH number	13	6	24	16	12	29	*.001*
Parietal lobe WMH number	6	3	10	9	3	13	*.018*
Temporal lobe WMH number	2	1	3	2	2	4	*.021*
Occipital lobe WMH number	1	1	2	2	1	3	*.471*
Deep white matter WMH number	15	6	27	19	13	33	*.001*
Subcortical WMH number	2	2	6	4	2	7	*.012*
Periventricular WMH number	3	1	4	4	1	4	*.021*
Callosal WMH number	2	1	5	3	1	5	*1.000*
Cerebral WMH volume (mL)	0.896	0.628	2.434	1.140	0.842	2.666	*.001*
Frontal lobe WMH volume (mL)	0.475	0.197	1.535	0.599	0.403	1.952	*.001*
Parietal lobe WMH volume (mL)	0.237	0.148	0.603	0.514	0.168	0.726	*.003*
Temporal lobe WMH volume (mL)	0.104	0.069	0.482	0.133	0.091	0.624	*.015*
Occipital lobe WMH volume (mL)	0.140	0.053	0.413	0.212	0.076	0.512	*.207*
Cerebral average WMH size (mL)	0.060	0.038	0.069	0.055	0.037	0.088	*.306*
Frontal lobe average WMH size (mL)	0.035	0.032	0.062	0.039	0.032	0.068	*.051*
Parietal lobe average WMH size (mL)	0.048	0.034	0.071	0.051	0.032	0.078	*.363*
Temporal lobe average WMH size (mL)	0.079	0.052	0.130	0.066	0.045	0.147	*.399*
Occipital lobe average WMH size (mL)	0.079	0.047	0.283	0.092	0.060	0.344	*.624*

ADC = apparent diffusion coefficient; Cho = choline compounds; Cr = creatine/phosphocreatine; Glx = glutamate/glutamine; mI = myo-inositol; NAA = N-acetyl-aspartate; NAWM = normal-appearing white matter; rCBF = relative cerebral blood flow; rCBV = relative cerebral blood volume; WMH = white matter hyperintensity.

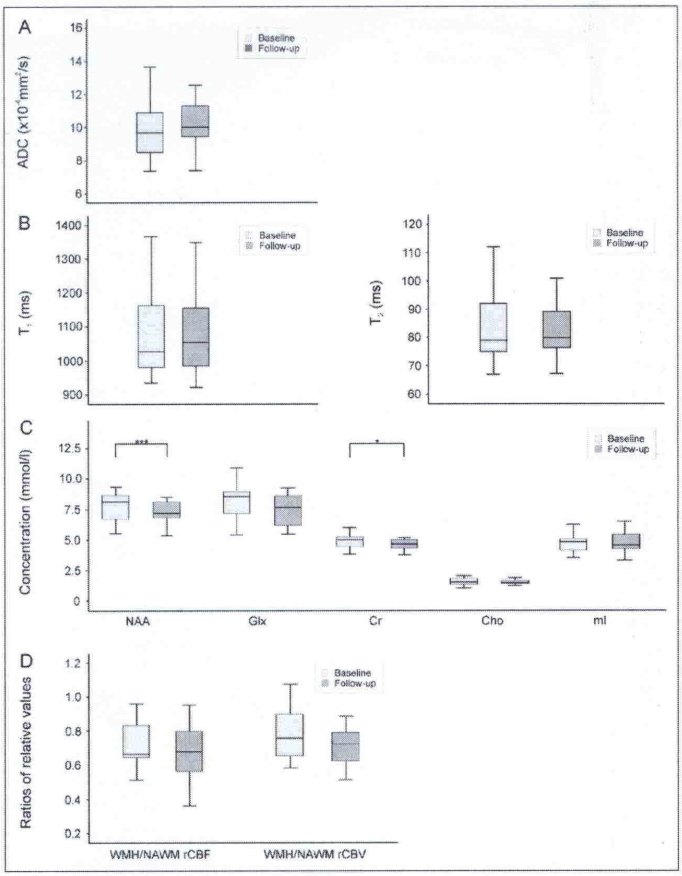

Fig 2.—Investigation of large brain white matter hyperintensities by different nonconventional magnetic resonance (MR) techniques. The graphs show differences between the baseline and the follow-up studies regarding the diffusion (A), the T1 and T2 relaxation time (B), the proton MR spectroscopy (C), and the perfusion (D) measurements. Whiskers are set at minimum and maximum, the horizontal line marks the median, whereas box indicates the interquartile range (25–75%). The statistically significant differences between the study groups are shown by * (*$P < .05$, ***$P < .001$). ADC = apparent diffusion coefficient; NAA = N-acetylaspartate; Glx = glutamate/glutamine; Cho = choline compounds, Cr = creatine/phosphocreatine, mI = myo-inositol; WMH = white matter hyperintensity, NAWM = normal-appearing white matter; rCBF = relative cerebral blood flow; rCBV = relative cerebral blood volume.

subcortical, periventricular, and corpus callosal locations (Table 3, Fig. 3B). In all locations, the hyperintensity number was higher in the follow-up study, with significant differences between the deep white matter ($P < .001$), the subcortical ($P = .012$), and the periventricular ($P = .021$) locations (Table 3, Fig. 3B). There was no correlation between the number of migraine attacks and the total number of hyperintensities (Spearman's correlation coefficient 0.465, $P = .097$). Out of 17 migraine patients, 16 patients had a higher number of WMHs in the follow-up study, while in 1 patient, the hyperintensity number remained unchanged (Table 1).

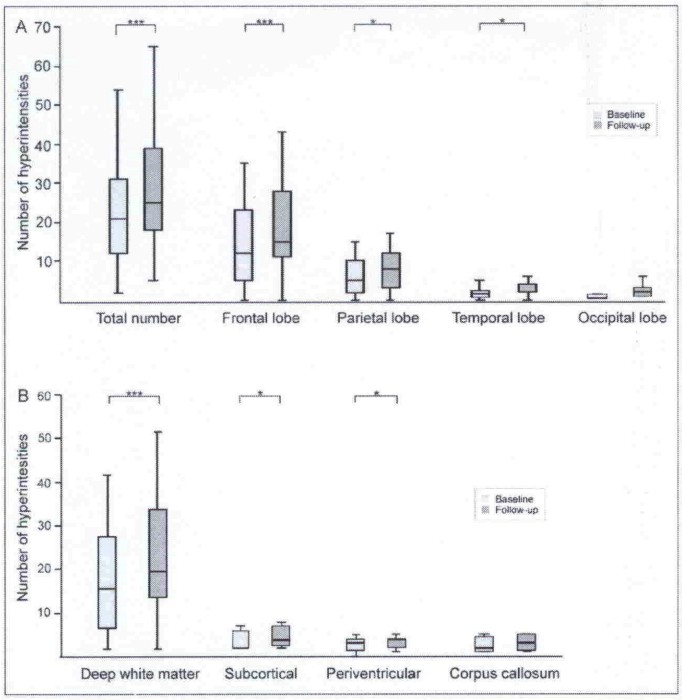

Fig 3.—The figure demonstrates differences in the hemispheric and lobar hyperintensity number between the baseline and the follow-up studies (A), and shows the intrahemispheric distribution and number of hyperintensities in four locations (B). Whiskers are set at minimum and maximum, the horizontal line marks the median, whereas box indicates the interquartile range (25–75%). The statistically significant differences between the groups are indicated by * on the figures (*$P < .05$, ***$P < .001$).

Cerebral and Lobar Volumes of WMHs.—WMHs were categorized based on their volumes. Compared to the baseline study, the cerebral and lobar volumes were larger at follow-up (Table 3). Except the occipital lobe, these differences were significant (cerebral $P < .001$, frontal $P < .001$, parietal $P = .003$, temporal $P = .015$; Table 3). A higher cerebral volume was found in all study patients at follow-up.

Cerebral and Lobar Average WMH Sizes.—The cerebral and lobar hyperintensity sizes were very similar in both studies, significant differences were not detected (Table 3).

Dynamic Properties of WMHs.—Dynamic properties of WMHs refer to any changes in their size (either decrease or increase), the development of new hyperintensities or the disappearance of old ones (Fig. 4).

Changes in Size of WMHs.—Most of the WMHs became larger after the 3-year long follow-up period (264 lesions, 67.7% of the WMHs observed at baseline, Table 4). All patients had at least 1 WMH with an increased volume (Table 1). Only the minority of WMHs had the same size at baseline and 3 years later (3.51% of hyperintensities detected at baseline, Table 4). A total of 91 WMHs had a smaller volume at follow-up (23.3%, Table 4) and all patients had at least 1 WMH that became smaller (Table 1). WMHs were categorized by their baseline volume. Hyperintensities smaller than the 33rd percentile were considered "small" (<0.034 mL) and hyperintensities larger than the 67th percentile were labeled as "large" hyperintensities (>0.059 mL) (Table 4). Hyperintensities between the 33rd and 67th percentiles were categorized as medium-sized

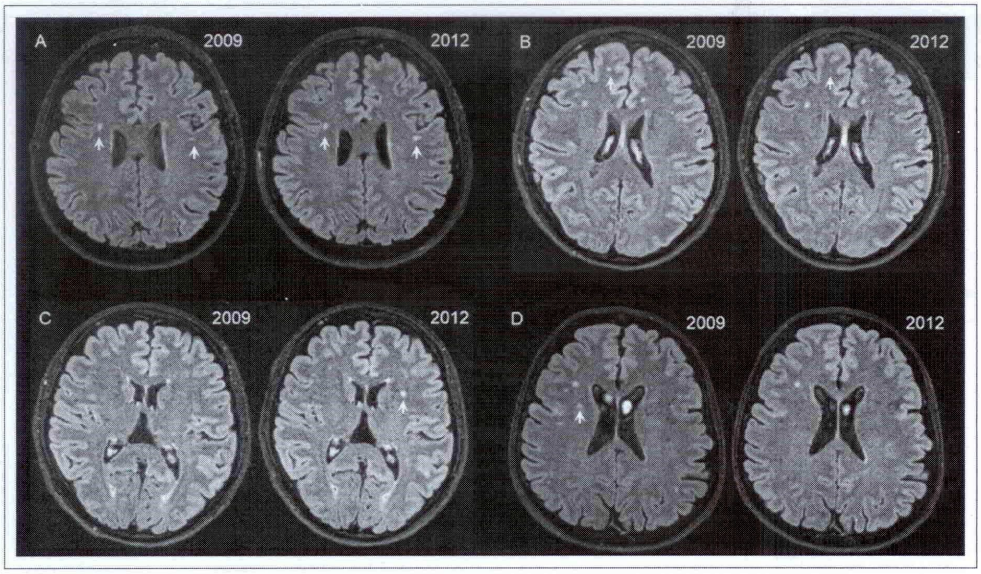

Fig 4.—Axial fluid-attenuated inversion recovery brain MRI images of 4 migraine patients. The images show changes between the baseline and the follow-up studies regarding the white matter hyperintensities. These include unchanged right frontal and larger left fronto-parietal bright signal intensities (A), smaller right frontal bright signal intensity (B), appearance of a new frontal hyperintensity (C), and a disappeared frontal hyperintense lesion (D). Images are presented in radiological convention (left = right).

hyperintensities (Table 4). Large hyperintensities significantly increased in size more often than medium-sized or small hyperintensities ($P < .002$; Table 5), while size decrease was most common in small hyperintensities ($P < .002$; Table 5). The number of increased or decreased-sized hyperintensities did not correlate with age, the disease duration, or the frequency of migraine attacks (correlation coefficients: 0.160, 0.360 and −0.470, $P > .05$, respectively).

Table 4.—Size-Dependent Distribution of White Matter Hyperintensities

	Number of WMHs			
WMH size range	Small 0-33 Percentile (<0.034 mL)	Medium-Sized 33-66 Percentile (0.034-0.059 mL)	Large 66-100 Percentile (>0.059 mL)	All_WMHs
Identical size	6	2	5	13
Increase in size	81	79	104	264
Decrease in size	26	41	24	91
Newly appeared	80	39	11	130
Disappeared	16	5	1	22

WMH = white matter hyperintensity.

Table 5.—Number and Volumetric Data of White Matter Hyperintensities With Size Change and Data of Newly Developed and Disappeared Hyperintensities

	WMHs With Increased Volume			WMHs With Decreased Volume			Wilcoxon Test (Bonferroni-Adjusted *P* value)	New WMHs			Disappeared WMHs			Wilcoxon Test (Bonferroni-Adjusted *P* value)
	Median	25th Percentile	75th Percentile	Median	25th Percentile	75th Percentile		Median	25th Percentile	75th Percentile	Median	25th Percentile	75th Percentile	
WMH number	14	9	19	5	3	7	*.004*	7	5	11	2	2	4	*.108*
Volume of all WMHs (mL)	0.233	0.16	0.632	0.050	0.026	0.062	*.002*	0.169	0.125	0.387	0.062	0.039	0.109	*.112*
Average WMH size (mL)	0.021	0.016	0.050	0.018	0.016	0.019	*.002*	0.030	0.018	0.036	0.032	0.020	0.039	*.116*

WMH = white matter hyperintensity.

Newly Developed and Disappeared WMHs.—The number of newly developed hyperintensities (n = 130) was higher than the number of disappeared ones (n = 22), (Tables 1, 4, and 5). Whereas 16 patients had at least 1 newly developed WMH, only 6 patients who had at least 1 disappeared WMH were identified (Table 1). The age of patients having disappeared WMHs ranged from 35-68 years (Table 1). The overall volumes of newly developed hyperintensities were higher compared to the volume of disappeared ones (Table 5). The average hyperintensity size of newly developed WMHs was similar to the average hyperintensity size of disappeared WMHs (Table 5), and most of these hyperintensities were small (Table 4). The number of newly developed hyperintensities did not correlate with age, the disease duration, or the frequency of migraine attacks (correlation coefficients: 0.196, 0.261, and −0.286, $P > .05$, respectively). While the number of disappeared hyperintensities did not correlate with the age and disease duration (correlation coefficients: −0.014 and 0.158, $P > .05$), the number of disappeared WMHs negatively correlated with the attack frequency at baseline (coefficient: −0.517, $P = .034$).

DISCUSSION

In the present study, we have reinvestigated a previously studied migraine group with brain WMHs performing the same quantitative MRI measurements 3 years after the initial study. In this homogenous migraine group, the recurrent headache attacks were the only known risk factors that could cause progression in the tissue impairment inside the WMHs or could lead to hyperintensity volume changes and the formation of new hyperintensities.

Evaluation of Large WMHs.—The reinvestigation of large WMHs with same anatomical coordinates demonstrated worsening in all migraine patients to differing degrees. Conversely, there were some migraineurs with the same or slightly improved values, although these were not uniformly seen in all the calculated measures (ADC, T1, and T2 relaxation time, ^{1}H-MRS, rCBF, rCBV). Progression in the large hyperintensities was found only in the ^{1}H-MRS study regarding the NAA and Cr concen-

trations. The baseline ^{1}H-MRS studies presented decreased NAA and Cr concentrations,[11] and the follow-up measurements showed a further reduction in the concentration of these metabolites. NAA is a neuronal/axonal marker, and its low concentration may reflect axonal loss with decreased viability and function.[24] Cr is a single resonance peak, containing signals from creatine and phosphocreatine, and the concentrations of these metabolites are higher in astrocytes and oligodendrocytes than in neurons.[24-26] Creatine is converted to phosphocreatine through the enzyme creatine kinase.[24] Phosphocreatine is a high-energy phosphate that is critical for maintaining cellular energy dependent systems.[24] The decreased brain levels of Cr can reflect tissue degeneration with low glial cellularity and less efficient mitochondrial functioning.[24-26]

Evaluation of All Cerebral WMHs.—The reinvestigation of migraine patients revealed a higher incidence of cerebral and lobar WMHs 3 years after the initial MRI study. The higher hyperintensity number associated with higher cerebral and lobar hyperintensity volumes. In concordance with previously reported data,[2,27-29] most of the hyperintensities were located in the deep white matter with the highest number in the frontal lobe. There was no difference between the baseline and the follow-up studies for the intracerebral distribution of lesions. Of the preexisting hyperintensities, 96.5% were not static in size, and the number of WMHs that increased in size was higher than those with a decreasing size. A higher number of newly developed hyperintensities were detected than disappeared hyperintensities, and the difference led to the increase of the cerebral hyperintensity count. The above-mentioned cerebral volume growth was related to both the number of new hyperintensities and the volume increase of preexisting ones. Most of the newly appeared and vanishing WMHs were small. The new hyperintensity group did not exclusively contain completely newly developed hyperintensities; there were previously seen hyperintensities that expanded to reach the predefined detection threshold, as well. Similarly, the vanishing hyperintensity group contained completely disappeared hyperintensities and shrunken hyperintensities that dipped below the minimum detectable size. The small hyperintensities were dynamically changing, whereas the medium-sized and large hyperintensities were more stable or progressive than regressive. It seems that in most of the WMHs, the original hyperintensity size predicts the probability of size increase or decrease. This finding confirms previous reports that the migraine-related WMHs cannot be just static or progressive, but the process can also be reversible.[30,31] The cause of these counter-moving hyperintensity changes is not known. If the nature of WMHs is ischemic, different types of vascular mechanisms and differences in the degree of tissue damage may explain these processes. In our previous[13] and present study, the ^{1}H-MRS measurements presented axonal damage with mitochondrial impairment within the hyperintensity. In the animal model of multiple sclerosis, spontaneously reversible inflammatory axon damage with intra-axonal mitochondrium pathology was discovered.[32] This mechanism may also be present in migraine giving an explanation for the regression of WMHs. Complete reversal of individual DWI hyperintensities was also found in small lesions of embolic stroke patients.[33]

We did not find any correlation between age, disease duration, and migraine attack frequency with the number of newly developed WMHs. Although the repeated headache attacks with different attack frequency may have a different impact on changes of white matter hyperintensities, the attack intensity and duration may be a factor with a greater impact than frequency alone. Conversely, a moderate negative correlation was found between the attack frequency and the number of disappeared hyperintensities. Based on these findings, we might assume that patients with disappeared hyperintensities had a low migraine attack frequency at baseline.

Our findings show that after a 3-year long follow-up period, new WMHs developed almost in all migraine patients, and most of the existing WMHs increased their volumes. The progressive nature of WMHs in migraine might be a result of the effects of repeated migraine attacks. This is supported by that a disappearance of WMHs were more commonly seen in patients with a low attack frequency compared to larger WMHs in patients with a

higher attack frequency. A prior longitudinal MRI study of migraineurs with a larger patient population and a longer follow-up period showed progression only in the incidence of deep white matter lesions in women,[28] whereas another longitudinal study detected no progression at all.[34] In these studies, the mean age of the patients was higher than in our study, and vascular risk factors were present in both patients and controls. In migraine patients with aura after a close to 3-year follow up, the WML number progressed over time.[35] In a recently published systematic review and meta-analysis of 6 population-based and 13 clinic-based studies,[7] the authors concluded that migraine may be a risk factor for structural brain changes including white matter abnormalities, infarct-like lesions, and volumetric changes in the gray and white matter regions. Since these studies varied in sample size, participant selection, headache characteristics, test methodology, timing of study, and data interpretation, the authors suggested additional longitudinal studies with a broad range of attack frequency and severity for better understanding the association between migraine and structural brain changes and to clarify the association to attack frequency and disease duration.

Study Limitations.—An important limitation of the present study is the small sample size, which is a consequence of the longitudinal design and strict selection criteria. Unfortunately, this sample size did not allow extensive correlation of WMH characteristics with clinical headache parameters including investigation of differences among migraine subgroups, neither did it allow us to control for potential confounding factors. Another important limitation is the lack of follow-up images of the original control group. Since healthy controls without headache matching the selection criteria did not have WMHs, such controls were not included in the study. Despite these limitations, our longitudinal analysis did identify predominantly progressive tendencies of WMHs, and most of these findings did remain significant even after Bonferroni adjustments to minimize type 1 error. Thus, although these results should not be generalized without caution, we believe they constitute a meaningful addition to the knowledge of WMHs in migraineurs, and we hope they would stimulate further research.

CONCLUSIONS

Although this follow-up study mainly showed worsening in the status of brain WMHs, occasional regression of these abnormalities was also observed in some cases. A lower baseline migraine attack frequency was associated with a tendency of decrease in WMH number at 3-year follow-up, implying a possible long-term relationship between the headaches and these imaging abnormalities. With the study limitations mentioned above, it should be noted that these findings cannot definitively differentiate between changes in WMHs due to migraine or possible changes that may occur through normal aging. However, further longitudinal studies can help to elucidate the nature of the relationship between migraine headaches and the MRI signal abnormalities found in these patients.

STATEMENT OF AUTHORSHIP

Category 1

(a) Conception and Design
Szilvia Erdélyi-Bótor, Anita Trauninger, Attila Schwarcz, Tamás Dóczi, Sámuel Komoly, Zoltán Pfund

(b) Acquisition of Data
Gabriella Deli, Anita Trauninger, Zoltán Pfund

(c) Analysis and Interpretation of Data
Mihály Aradi, David Olayinka Kamson, Gábor Perlaki, Gergely Orsi, Szilvia Anett Nagy, Norbert Kovács, Zoltán Pfund, Szilvia Erdélyi-Bótor

Category 2

(a) Drafting the Manuscript
Szilvia Erdélyi-Bótor, David Olayinka Kamson, Gábor Perlaki, Gergely Orsi, Zoltán Pfund

(b) Revising It for Intellectual Content
Szilvia Erdélyi-Bótor, David Olayinka Kamson, Attila Schwarcz, Tamás Dóczi, Sámuel Komoly, Zoltán Pfund

Category 3

(a) Final Approval of the Completed Manuscript
Attila Schwarcz, Tamás Dóczi, Sámuel Komoly, Anita Trauninger, Zoltán Pfund

REFERENCES

1. Headache Classification Committee of the International Headache Society. The International Classification of Headache Disorders, 2nd edn. *Cephalalgia*. 2004;24(Suppl. 1):1-160.
2. Kruit MC, van Buchem MA, Hofman PA, et al. Migraine is a risk factor for subclinical brain lesions. *JAMA*. 2004;291:427-434.
3. Kruit MC, Launer LJ, Ferrari MD, van Buchem MA. Infarcts in the posterior circulation territory in migraine. The population-based MRI CAMERA study. *Brain*. 2005;128:2068-2077.
4. Kruit MC, Launer LJ, Ferrari MD, van Buchem MA. Brain stem and cerebellar hyperintense lesions in migraine. *Stroke*. 2006;37:1109-1112.
5. Kruit MC, van Buchem MA, Launer LJ, Terwindt GM, Ferrari MD. Migraine is associated with an increased risk of deep white matter lesions, subclinical posterior circulation infarcts and brain iron accumulations: The population-based MRI CAMERA study. *Cephalalgia*. 2010;30:129-136.
6. Kurth T, Mohamed S, Maillard P, et al. Headache, migraine, and structural brain lesions and function: Population based Epidemiology of Vascular Ageing-MRI study. *BMJ*. 2011;342:c7357.
7. Bashir A, Lipton RB, Ashina S, Ashina M. Migraine and structural changes in the brain: A systematic review and meta-analysis. *Neurology*. 2013;81:1260-1268.
8. Fazekas F, Koch M, Schmidt R, et al. The prevalence of cerebral damage varies with migraine type: A MRI study. *Headache*. 1992;32:287-291.
9. De Benedittis G, Lorenzetti A, Sina C, Bernasconi V. Magnetic resonance imaging in migraine and tension-type headache. *Headache*. 1995;35:264-268.
10. Schmitz N, Admiraal-Behloul F, Arkink EB, et al. Attack frequency and disease duration as indicators for brain damage in migraine. *Headache*. 2008;48:1044-1055.
11. Trauninger A, Leél-Őssy E, Kamson DO, et al. Risk factors of migraine-related brain white matter hyperintensities: An investigation of 186 patients. *J Headache Pain*. 2011;12:97-103.
12. Bednarczyk EM, Remler B, Weikart C, Nelson AD, Reed RC. Global cerebral blood flow, blood volume, and oxygen metabolism in patients with migraine headache. *Neurology*. 1998;50:1736-1740.
13. Aradi M, Schwarcz A, Perlaki G, et al. Quantitative MRI studies of chronic brain white matter hyperintensities in migraine patients. *Headache*. 2013;53:752-763.
14. Oppenheimer SM, Bryan RN, Conturo TE, Soher BJ, Preziosi TJ, Barker PB. Proton magnetic resonance spectroscopy and gadolinium-DTPA perfusion imaging of asymptomatic MRI white matter lesions. *Magn Reson Med*. 1995;33:61-68.
15. Zivadinov R, Bergsland N, Stosic M, et al. Use of perfusion- and diffusion-weighted imaging in differential diagnosis of acute and chronic ischemic stroke and multiple sclerosis. *Neurol Res*. 2008;30:816-826.
16. Zhu YC, Dufouil C, Tzourio C, Chabriat H. Silent brain infarcts: A review of MRI diagnostic criteria. *Stroke*. 2011;42:1140-1145.
17. Young VG, Halliday GM, Kril JJ. Neuropathologic correlates of white matter hyperintensities. *Neurology*. 2008;71:804-811.
18. Kamson DO, Illés Z, Aradi M, et al. Volumetric comparisons of supratentorial white matter hyperintensities on FLAIR MRI in patients with migraine and multiple sclerosis. *J Clin Neurosci*. 2012;19:696-701.
19. Provencher SW. Automatic quantitation of localized in vivo ^{1}H spectra with LCModel. *NMR Biomed*. 2001;14:260-264.
20. Vermeer SE, Hollander M, van Dijk EJ, Hofman A, Koudstaal PJ, Breteler MMB. Silent brain infarcts and white matter lesions increase stroke risk in general population. *Stroke*. 2003;34:1126-1129.
21. 3D Slicer. 3D Slicer website 2010. http://slicer.org/ accessed September 27, 2010.
22. Jenkinson M, Bannister P, Brady M, Smith S. Improved optimization for the robust and accurate linear registration and motion correction of brain images. *Neuroimage*. 2002;17:825-841.
23. Smith SM, Zhang Y, Jenkinson M, et al. Accurate, robust, and automated longitudinal and cross-sectional brain change analysis. *Neuroimage*. 2002;17:479-489.
24. Moore GJ. Proton magnetic resonance spectroscopy in pediatric neuroradiology. *Pediatr Radiol*. 1998;28:805-814.
25. Barkhof F, van Walderveen M. Characterization of tissue damage in multiple sclerosis by nuclear magnetic resonance. *Philos Trans R Soc Lond B Biol Sci*. 1999;354:1675-1686.

26. Mader I, Rauer S, Gall P, Klose U. ^{1}H MR spectroscopy of inflammation, infection and ischemia of the brain. *Eur J Radiol*. 2008;67:250-257.
27. Rossato G, Adami A, Thijs VN, et al. Cerebral distribution of white matter lesions in migraine with aura patients. *Cephalalgia*. 2010;30:855-859.
28. Palm-Meinders IH, Koppen H, Terwindt GM, et al. Structural brain changes in migraine. *JAMA*. 2012;308:1889-1897.
29. Seneviratne U, Chong W, Billimoria PH. Brain white matter hyperintensities in migraine: Clinical and radiological correlates. *Clin Neurol Neurosurg*. 2013;115:1040-1043.
30. Rozen TD. Vanishing cerebellar infarcts in a migraine patient. *Cephalalgia*. 2007;27:557-560.
31. Rozen TD. Images from headache: White matter lesions of migraine are not static. *Headache*. 2010; 50:305-306.
32. Nikić I, Merkler D, Sorbara C, et al. A reversible form of axon damage in experimental autoimmune encephalomyelitis and multiple sclerosis. *Nat Med*. 2011;17:495-499.
33. Albach FN, Brunecker P, Usnich T, et al. Complete early reversal of diffusion-weighted imaging hyperintensities after ischemic stroke is mainly limited to small embolic lesions. *Stroke*. 2013; 44:1043-1048.
34. Hamedani AG, Rose KM, Peterlin BL, et al. Migraine and white matter hyperintensities: The ARIC MRI study. *Neurology*. 2013;81:1308-1313.
35. Dinia L, Bonzano L, Albano B, et al. White matter lesions progression in migraine with aura: A clinical and MRI longitudinal study. *J Neuroimaging*. 2013;23:47-52.